A STUDY OF THE EFFECTS OF THE MICRO-CHANNEL COLD PLATE ON THE COOLING PERFORMANCE OF BATTERY THERMAL MANAGEMENT SYSTEMS

by

Zhen GONG[a], Hao TANG[a,b,c*], and Yu WANG[a]

[a] College of Energy and Power Engineering,
Nanjing University of Aeronautics and Astronautics, Nanjing, China
[b] Nanjing University of Aeronautics and Astronautics,
Aero-Engine Thermal Environment and Structure Key Laboratory of
Ministry of Industry and Information Technology, Nanjing, China
[c] Nanjing University of Aeronautics and Astronautics,
Jiangsu Province Key Laboratory of Aerospace Power System, Nanjing, China

Original scientific paper
https://doi.org/10.2298/TSCI210608316G

Li-ion batteries are widely used in electric vehicles for their superior performance. To investigate a simple and efficient method for the Li-ion power batteries, the cold plate with four types of structures A, B, C, and D were established, respectively. Subsequently, the effects of micro-channel thickness and width on the cooling performance of battery thermal management systems were analyzed by using a numerical simulation method. The results show that with the increases of the micro-channel thickness, the maximum temperature, T_{max}, of the cold plate is gradually increased under structures A, B, and C, while it is gradually decreased under structure D. The standard deviation of temperature, T_{σ}, of the cold plate of structure A was less affected by the change of the micro-channel thickness. Under structures B, C, and D, the temperature uniformity of the cold plate can be well maintained when the micro-channel thickness was 1.0 mm. With the increase of the micro-channel width, the T_{max} and T_{σ} of the cold plate are gradually increased in all cases, while the ΔP from the inlet to outlet is gradually decreased. The temperature uniformity of the cold plate is well maintained by structure C. The decreasing amount and changing range of ΔP caused by the change of micro-channel width is smaller than caused by the change of the thickness.

Key words: *micro-channel, cold plate, temperature, thickness, width*

Introduction

In recent years, the energy crisis and global warming have become more and more serious [1]. Therefore, the development and utilization of clean energy in various industry departments are becoming mainstream [2]. Among them, conventional internal combustion vehicle is regarded as the major cause for the growing issue of energy crisis and environmental pollution. To alleviate global energy and environmental problems, countries around the world are developing clean energy vehicles actively to replace traditional internal combustion vehicles [3].

Nowadays, clean energy vehicles mainly include pure electric vehicles (EV), hybrid electric vehicles (HEV), and plug-in hybrid electric vehicles (PHEV) which have advantages of environmentally friendly and energy-saving compared with traditional internal combustion

* Corresponding author, e-mail: hao.tang@nuaa.edu.cn

vehicles [4]. Among the aforementioned clean energy vehicles, the EV will be developed rapidly in the future due to their advantages of simple structure, low production cost, and no exhaust emissions. The battery is one of the core components of EV, the safety and stability of EV will be directly affected by their quality. Li-ion batteries are widely used in the field of EV due to their advantages of high energy density, high power density, long life, environmental friendliness, and fast charging rate [5, 6].

However, Li-ion batteries generate a large amount of heat during operation, which can accelerate the battery's aging process, causes uneven temperature distribution, even causes an explosion if the heat of batteries cannot be dissipated in time [7]. Studies showed that the optimal temperature range of Li-ion batteries is 15~35 ℃, and the temperature difference of the battery cells cannot exceed 5 ℃. Therefore, to ensure the best performance of Li-ion batteries, the battery thermal management system (BTMS) will be installed in EV [8].

Nowadays, the BTMS mainly includes forced convection with air cooling, liquid cooling, and phase change cooling [9-11]. Among these types, forced air cooling is the most commonly used due to its simple structure and high security for the battery packs [12]. However, air cooling also has the disadvantage of low heat transfer coefficient, which can cause the non-uniform distribution, especially for the high-rate discharge process of the battery [13]. In addition, the phase change cooling technology is not yet mature and the cooling effect cannot be controlled well [14]. Compared with air cooling and phase change cooling, liquid cooling is the best one among the mainstream cooling methods, due to it has advantages of high cooling efficiency and uniform cooling effect. To prevent the battery from short-circuiting in the liquid, the battery's cells are usually not in direct contact with the cooling liquid when using liquid cooling. Therefore, the use of micro-channels cooling plates in liquid cooling is a batter cooling method [15]. In recent years, more and more people paying attention to the research of micro-channels plates.

Tang *et al.* [16] proposed a cooling strategy for Li-ion battery packs by using the micro-channels cooling plate and designed three types of the mini-channels cold plate. The feasibility of this strategy is verified by a combination of experiments and numerical simulation. Lee *et al.* [17] designed a *U*-shaped micro-channel cold plate and the effects of discharge rate, inlet mass-flow rate, and operating temperature on the cooling performance of Li-ion batteries were studied respectively. Deng *et al.* [18] designed a cold plate of serpentine-channel configuration to study the effects of the number of channels, the layout channels, and coolant inlet flow on the cooling performance of the battery. The results showed that the best cooling performance of the cold plate was obtained when the number of channels was 5. Lan *et al.* [19] designed a micro-channel cold plate on a prismatic Lin-ion battery cell. They figure out the effects of discharge rate, velocity distribution, and operating temperature on battery thermal management performance. Therefore, an effective BTMS to cool down the prismatic Li-ion batteries by cold plate is still needed to be further developed, and the efficient and safer BTMS safe is highly desired.

The layout of micro-channels in the cold plate has a great influence on the performance of BTMS, and the temperature rise of the clod fluid in the working process will cause the reduction of its heat exchange capacity, which leads to the uneven temperature distribution on the battery. Hence, in this paper, a dual-channel layout is proposed, and the existing two cold plates models are improved, and the cooling performance of the clod plate before and after the improvement is compared by numerical simulation software (ANASYS FLUENT). The main aim of the present work is to guide the design of a thermal management system for large-capacity rectangular batteries.

Model establishment

Geometric models

In this paper, the micro-channels cold plate is mainly used for rectangular Li-ion batteries. The cold plate is mainly installed between two adjacent battery cells and the outermost of the battery cells, as shown in fig. 1. Large heats are generated in the Lin-ion battery during charging and discharging, which is conducted into the cold plate, and then the heat is transmitted by the cooling liquid, hence the battery cells are cooled.

As shown in fig. 1, the length and height of the micro-channel cold plate are the same as the battery cells. Aluminum was chosen to be the material of the cold plate, and water was used as the cooling liquid. The A, B, C, and D, four types of cold plate structures are designed as shown in figs. 2(a)-2(d). The single flowing channel is adopted by the structures A and C, and double flowing channels, the double channels have opposite liquid flow directions, are adopted by the structures B and D. As the cold plate between two adjacent batteries is symmetrical in the thickness direction, hence, a half cold plate can be studied to shorten computing time, and the symmetry plane is set at the center of the cold plate.

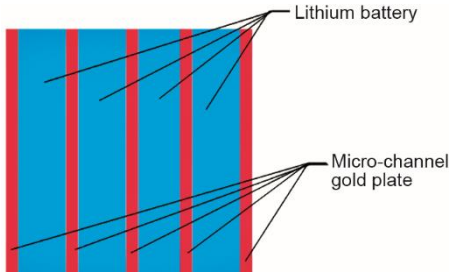

Figure 1. The schematic diagram of micro-channel cold plate installation

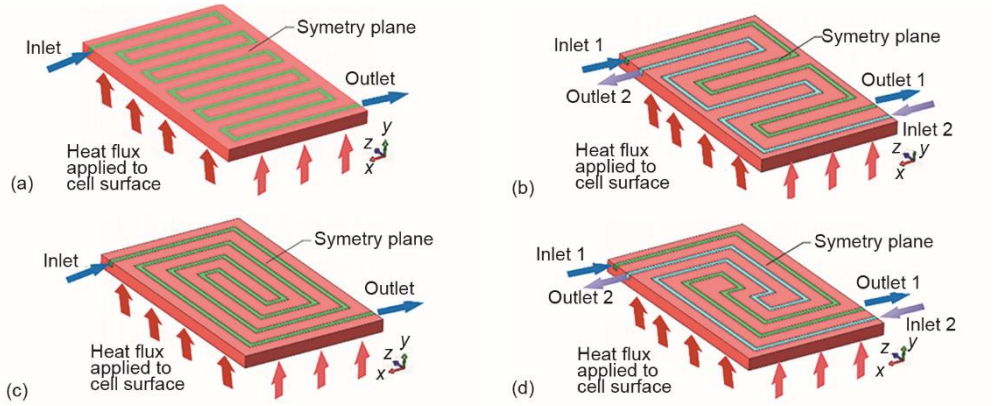

Figure 2. The schematic diagram of the central cross-sectional structure of the cold plate

The length, height, and thickness of the cold plate are set to 115, 180, and 2 mm, respectively, and the total lengths of the micro-channel are set to 1185 mm in all structures. The thicknesses of the cold plate are reduced to 1 mm after the symmetry planes on the geometric model are applied. To study the effects of width and thickness of micro-channel on the cooling performance, the widths of the micro-channels are set to 4, 5, 6, and 7 mm when the thickness of the micro-channel is 0.6 mm, respectively, and the thicknesses of micro-channels are set to 0.6, 0.8, 1.0, and 1.2 mm when the width of micro-channel is 0.6 mm, respectively. After the symmetry condition was applied, the thicknesses of micro-channels are reduced to 0.3, 0.4, 0.5, and 0.6 mm, respectively. The cross-sectional area of the liquid flow channel will be changed when the width and thickness of the micro-channel were changed. Therefore, to maintain the heat balance between the inlet and outlet of the cooling liquid, the constant

mass inlet is set at the cooling liquid inlet. The inlet flow of the structures A and C are set to $2 \cdot 10^{-3}$ kg/m, and each inlet flow of the structures B and D are set to $1 \cdot 10^{-3}$ kg/m. Note that the inlet flow has been reduced to half of the original after the symmetry condition was applied. The pressure outlets of all cases are applied at the cooling liquid outlet.

The maximum Reynolds number during the cooling liquid flow is calculated to be 1702.5, and the Reynolds number below 2300. Hence, the laminar model is selected in numerical simulation.

In this paper, the Li-ion battery has a capacity of 12.9 Ah and a nominal voltage of 3.2 V, and the discharge power is 41.28 W. To study the effects of the micro-channel structure on the battery at a 1C discharge rate, the uniform heat flux of 1000 W/m^2 is applied through the surface of the cold plate, as shown in fig. 2. The cold plates are assumed to be homogenous and isotropic for numerical simplicity. The natural convection heat transfer coefficients of the four outer walls of the cold plate are set to 2 W/m^{2}K, and all operating temperatures are set as 25 ℃. The detailed analysis parameters of numerical simulation are given in tab. 1.

Table1. Detailed analysis parameters of numerical simulation

Material properties	Value	Unit
Cooling liquid	Liquid water	–
Liquid density	998.2	[kgm^{-3}]
Liquid specific heat	0.4182	[Jkg^{-1}k^{-1}]
Liquid viscosity	0.001003	[kgm^{-1}s^{-1}]
Cold plat material	Aluminum	–
Cold plate density	2719	[kgm^{-3}]
Cold plate specific heat	871	[Jkg^{-1}k^{-1}]
Cold plate conductivity	202.4	[Wm^{-1}k^{-1}]
Dimensions		
Cold plate thickness	2	[mm]
Cold plate height	180	[mm]
Cold plate length	115	[mm]
Channel thickness	0.6, 0.8, 1.0, 1.2	[mm]
Channel width	4, 5, 6, 7	[mm]
Channel total length	1185	[mm]
Boundary conditions	—	—
Inlet mass flow rate	$2 \cdot 10^{-3}$	[kgs^{-1}]
Operating temperature	25	[℃]
Heat flux	1000	[Wm^{-2}]
Wall convection heat transfer coefficient	2	[Wm^{-2}K^{-1})
Flow model	Laminar	–

To better evaluate the cooling performance of micro-channel cold plate, the maximum temperature, T_{max}, temperature difference, T_{diff}, the standard deviation of temperature, T_σ, of the cold plate surface, and the total pressure drop between inlet and outlet, ΔP, were

monitored during the simulation. The T_{max} and T_{diff} can reflect the most severe working condition of batteries, the T_{diff} is defined as the difference between the maximum and minimum surface temperatures. The ΔP can reflect the pressure difference between the inlet and outlet cooling liquid, and the larger the ΔP is, the higher the energy consumed by the pump to maintain the flow of the liquid. The T_σ implies the uniformity of temperature distribution for battery cells. The smaller T_σ means more uniform distribution of temperature on batteries.

Mesh generation

The FLUENT meshing was used to mesh the models, and polyhedral grids were used in both fluid and solid regions. Structure A was used to verify the mesh independence of the model when the thickness and width of the micro-channel were 0.6 mm and 4 mm, respectively. The number of 304633 cells, 408256 cells, 508964 cells, 623215 cells, and 732562 cells volume mesh is divided respectively by changing the mesh size. The T_{max} of the cold plate is monitored during the simulation. The T_{max} variations curve under different volume numbers is shown in fig. 3.

As can be seen in fig. 3, with the increase of the number of volume mesh, the T_{max} showed a trend of gradual decrease. However, the T_{max} is decreased slightly when the volume mesh number exceeds 508964 cells, hence, it can be considered that when the number of volume mesh is 508964 cells, the temperature variation performance of the cold plate can be better simulated. Therefore, the meshing method is adopted during the simulation.

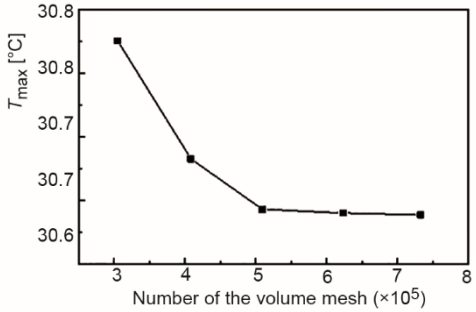

Figure 3. Independence checking of the volume mesh

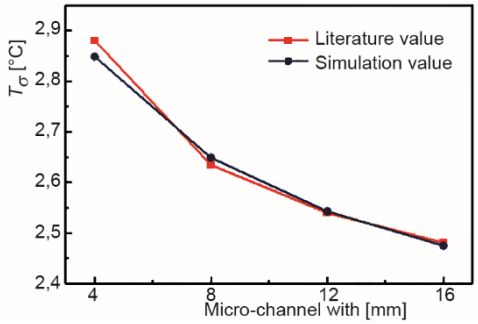

Figure 4. The comparison results between simulation and literature

Method validation

The model in literature [20] was simulated using the explained method, and the results of T_σ under different micro-channels widths were compared with those in the literature, the comparison results are shown in fig. 4. As can be seen in fig. 4, the simulation values are in good agreement with those in the literature, which shows that the method adopted in this paper can well simulate the temperature distribution of the cold plate.

Results and discussion

The analysis of thermal management performance of micro-channel cold plates with different structures

To study the thermal management performance under different cold plate structures, the A, B, C, and D four structures cold plates were simulated, respectively. The width and thickness of the micro-channel are set to 4 mm and 0.6 mm, respectively. The temperature

distributions of the contact surface between the cold plates and the battery cells are shown in figs. 5(a)-5(d).

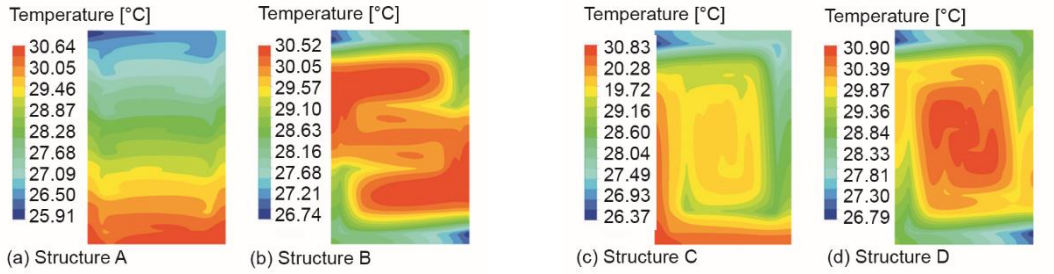

Figure 5. Temperature distributions of the contact surface between the cold plates and the battery cells (*for color image see journal web site*)

It can be seen from fig. 5 that the temperature distributions have great differences under the four structures. The temperature distribution of structure A shows a gradually increasing trend from top to bottom. The inlet and outlet of cooling liquid under structure A are located at the upper and lower parts of the cold plate, respectively. As the cooling liquid flows from the inlet to the outlet, the heat is absorbed by the cooling liquid, which the temperature of the cooling liquid is increased. Meanwhile, the temperature difference between the cooling liquid and the cold plate is decreased gradually, which leads to the cooling capacity of the cooling liquid is decreased. Hence, the temperature distribution of structure A shows a trend of gradual increase from top to bottom.

The temperature distribution under structure B shows a trend that the upper and lower parts of the cold plate are lower and the middle parts of the cold plate are higher, and the distribution of the high temperature area is S-shaped. Compared with structure A, structure B has a larger high temperature area, and the temperature gradient at the inlet of the cooling liquid is increased significantly.

The high temperature area of structure C is mainly distributed at the left edge and the bottom edge region of the cold plate, and the high temperature area is smaller than the other three structures. Because the left edge and the bottom edge region of the cold plate are close to the outlet of the micro-channel, and the cooling capacity of the liquid at this position is reduced, hence the high temperature areas are formed at these parts.

The high temperature area of structure D is mainly concentrated in the center region of the cold plate. It can demonstrate that the central region of the cold plate cannot be well cooled under structure D.

Figures 6(a)-6(c) show the change curves of T_{max}, T_{diff}, and T_{σ}, respectively, under different cold plate structures. Figures 6(a) and 6(b) can be seen that both T_{max} and T_{diff} in structure B are the lowest. It can demonstrate that the most severe working condition of batteries can be well controlled by structure B. It is worth noting that the T_{max} in structure A is only higher than that the structure B, but the T_{diff} is the largest in all cases. It shows that structure A can better control the maximum temperature of batteries, but the performance of controlling the temperature difference of batteries is poor. The T_{max} of the structure C and D are close to each other, both of which are about 30.9 °C, but the T_{diff} of the structure D is about 0.05 °C lower than that of the structure C. It is indicating that the performance of temperature control of structure D is better than that of structure C.

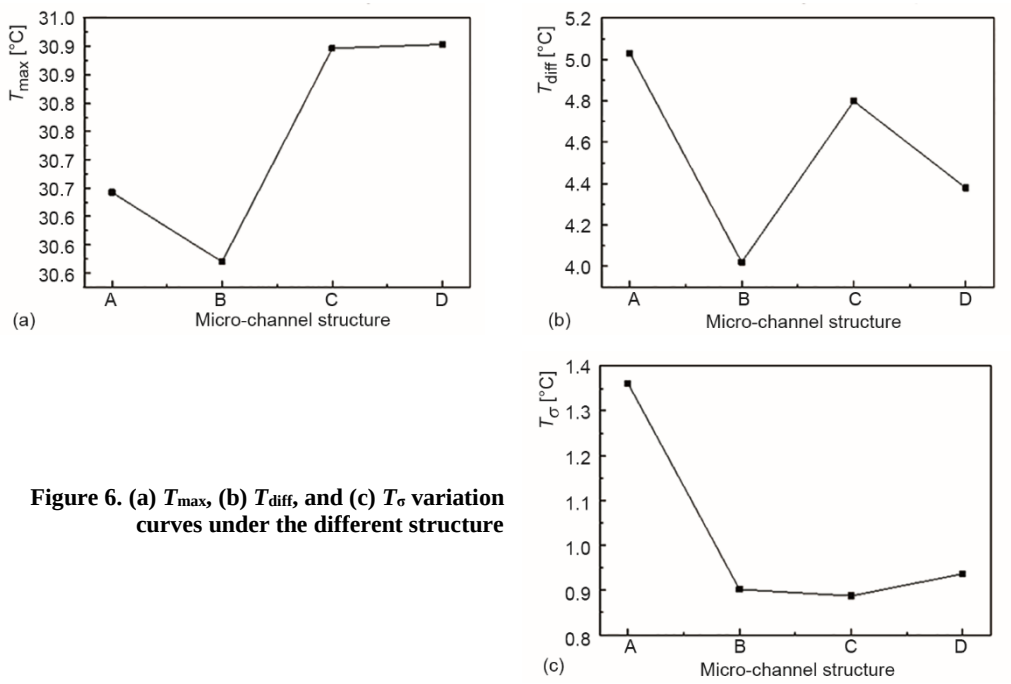

Figure 6. (a) T_{max}, (b) T_{diff}, and (c) T_σ variation curves under the different structure

According to fig. 6(c), it can be seen that the T_σ in structure A is the largest in all cases, it indicated that structure A has the worst performance of maintaining temperature uniformity of battery cell. The T_σ in the structures B, C, and D are only slightly different, it indicated that the temperature uniformity of battery cells can be well maintained by the structures B, C, and D.

The ΔP variations curves under different structures are shown in fig. 7. It is worth noting that the ΔP of structures A and C are close to each other, and the ΔP of the structures B and D are also close to each other, and the ΔP value of the structures A and C are much higher than those of the structures B and D. This can explain that the pressure loss of cooling liquid can be effectively reduced by the dual-inlet method under the same total mass flow, which the energy consumption to maintain the stable flow of the cooling plate are reduced.

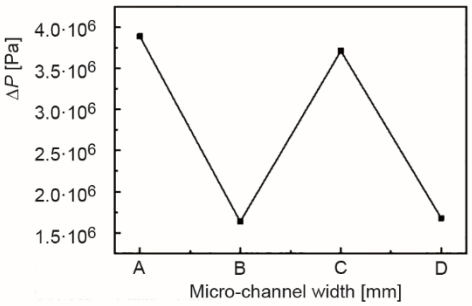

Figure 7. The ΔP variations curve under the different structure

The pressure loss of the fluid is mainly caused by the linear loss, P_f, and local loss, P_m, in the flow process. The linear loss is mainly affected by the length of the flow channel, l, the equivalent diameter of the flow channel, D_d, the fluid velocity, v, the fluid density, ρ, and the linear loss coefficient, λ. The linear loss can be expressed:

$$P_f = \lambda \frac{l}{D_d} \frac{\rho v^2}{2} \tag{1}$$

The P_m is mainly caused by local resistance. The local loss of micro-channel designed in this paper mainly occurs at the corner of the flow channel. The local loss is mainly affected by fluid velocity, v, the fluid density, ρ, and the local loss coefficient, ζ. The local loss can be expressed:

$$p_m = \zeta \frac{\rho v^2}{2} \tag{2}$$

It can be seen that although the total micro-channel length of dual-inlet is the same as that of the single-inlet, while the flow rate of the cooling liquid is reduced to one half of that of the single inlet, hence, theoretically, the pressure drop under the same condition is reduced to 1/4 of that the single-inlet. Therefore, leads to the ΔP of structures A and C is higher than that of structures B and D.

However, it can be known from the simulation results that the ΔP value of structures A and C are about 2/5 of the structures B and D, which is larger than the theoretical value. The reason for this phenomenon is that structures A and C have more parts that cause the cooling liquid direction to be changed than the structures B and D, which caused the local loss of the structures A and C are greater.

The analysis of thermal management performance of cold plates with different micro-channel thicknesses

The temperature distributions of the structures A, B, C, and D, under different thicknesses of micro-channel are shown in figs. 8(a)-8(d), respectively, (the micro-channels widths are maintained constant at 4 mm).

According to fig. 8, it is seen that the high temperature area of the cold plate under the structures A, B, and C gradually expands with the increase of the thickness of micro-channels, and the lower temperature areas are decreased gradually at the same time. This may be because the cross-sectional areas of the micro-channel are increased with the gradual increase of the thickness of the micro-channel, which the flow velocity of cooling liquid is decreased gradually under the condition of constant mass-flow, hence, the temperature of the cooling liquid will be raised for the same distance. As the temperature of the cooling liquid increases, the cooling capacity of the cooling liquid is gradually decreased. Therefore, the high temperature area of the cold plates under the structure A, B, and C gradually expands with the increase of the thickness of micro-channels. However, as shown in fig. 8(d), the high temperature areas in the center region of the structure of D are gradually decreased with the increase of thickness of micro-channels. The reason for this phenomenon is that the distance from the inlet of the cooling liquid to the center part of the cold plate is short under the structure D and the total volume of the micro-channel is increased when the increase of micro-channel thickness. Hence, as the thickness of the increases of micro-channels, the cooling liquid in the cold plate is increased, the more heat of the center of parts of the cold plate is absorbed by the cooling liquid. Therefore, results in the high temperature areas in the center of the cold plate of the structure D are decreased.

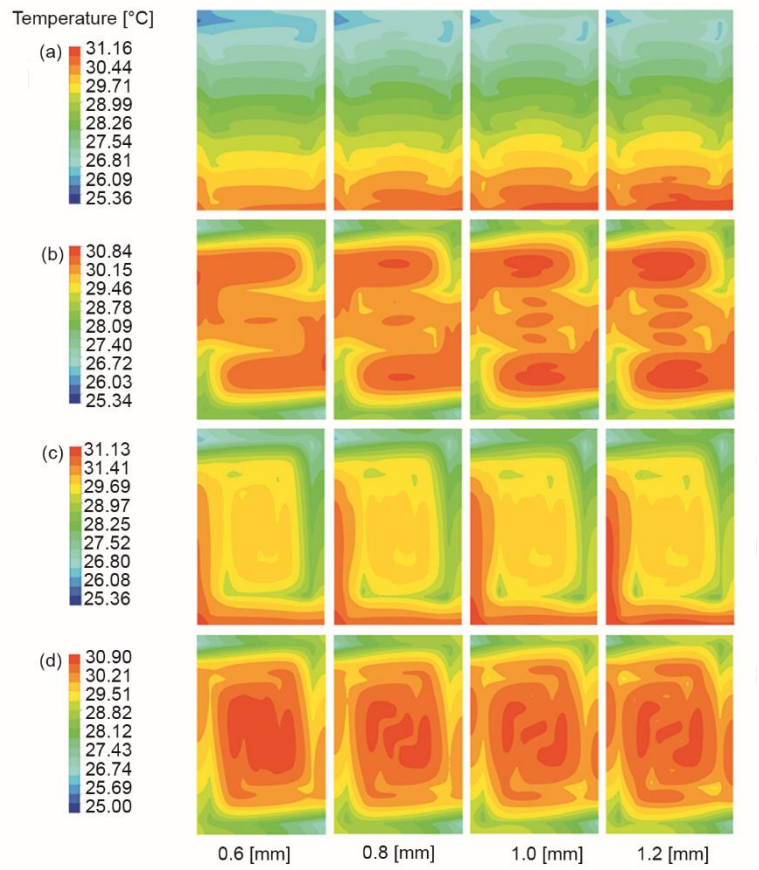

Figure 8. The temperature distributions under different thicknesses of micro-channel (*for color image see journal web site*)

The variation curves of T_{max}, T_{diff}, and T_{σ} with the thickness of micro-channels are shown in figs. 9(a)-9(c), respectively. As shown in fig. 9(a), with the increases of the thickness of micro-channels, the T_{max} is gradually increased under the structures A, B, and C, while it shows a trend of gradual decrease under structure D. As discussed previously, the variations trends of the T_{max} are similar to that of the high temperature area of the cold plate. With the increase of the high temperature area, the heat transfer in the center of the high temperature area is inhibited, which causes the maximum temperature of the region to be raised. On the contrary, the heat transfer capacity in the center of the high temperature area is increased when the decrease of the high temperature area, which the maximum temperature of the region is reduced. As shown in fig. 9(b), with the increases of the thickness of the micro-channel, the T_{diff} under structure A shows a trend of gradual increase, while it shows a trend of gradually decreasing first and then stabilizing under the structures B, C, and D. In structure A, the cross-sectional area of the micro-channel is increased due to the increase of the thickness of micro-channels, which the flow velocity of the cooling liquid is decreased. Afterward, the temperature at the bottom of the cold plate is increased, and meanwhile, the temperature at the inlet of the cooling liquid is kept essentially constant, hence, the T_{diff} has shown a trend of

gradually increasing. Based on the above analysis, it can be concluded that structure A has a poor ability to maintain the temperature difference of the cold plate compared with the other three structures.

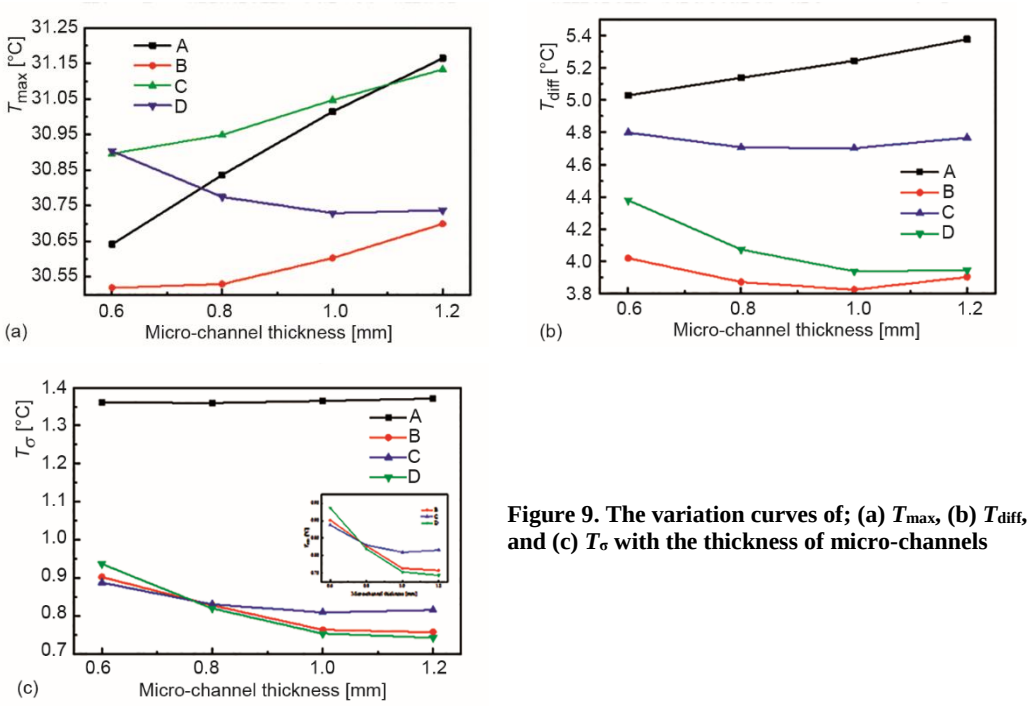

Figure 9. The variation curves of; (a) T_{max}, (b) T_{diff}, and (c) T_σ with the thickness of micro-channels

As shown in fig. 9(c), in structure A, the T_σ values of the cold plates are greater than 1.35 in all cases and it is significantly higher than the other three structures, and a slight increase in T_σ value can be observed as the thickness of the micro-channel increases. The result demonstrates that the temperature uniformity of the cold plate cannot be well maintained under structure A, and it is less affected by the change of thickness of the micro-channels. Compared to structure A, the T_σ values of the cold plate under structures B, C, and D are decreased obviously with the increase of thickness of the micro-channels. Under structures B, C, and D, the decrease of T_σ of the cold plate are significantly when the thickness of micro-channels is increased from 0.6 mm to 1.0 mm, while it is relatively slower when the thickness of micro-channels is increased to 1.2 mm. Hence, it can be concluded that the temperature uniformity of the cold plate can be well maintained when the thickness of the micro-channel is 1.0 [mm] under structures B, C, and D.

Figure 10 shows the variations curves of ΔP with the thickness of the micro-channel. It is clearly seen that the ΔP of structures A and C is higher than that of structures B and D under the same thickness of micro-channels. Hence, it can be concluded that the pressure loss of cooling liquid from inlet to outlet of the micro-channel can be effectively reduced by using the dual-inlet structure. As shown in fig. 10, the ΔP of the four structures are all decreased with the increase of thickness of the micro-channel, moreover, it is worth noting that with the thickness of the micro-channel increase, the decreases of the ΔP become smaller when the micro-channel increases the same thickness. There are two main reasons for this phenomenon. On the hand, the flow velocity of the cooling liquid in the micro-channel is de-

creased, while the equivalent diameter of the micro-channel is increased. According to eq. (1), both the decrease of flow velocity and the increase of equivalent diameter can reduce the linear loss. On the other hand, the thickness of the micro-channel is set as an independent variable due to only the thickness of the micro-channel makes the change in all cases of this section, afterward, the quadratic differentiation of eq. (1) shows that the result is always greater than 0, which eq. (1) is a concave function when the thickness is an independent variable. Hence, the decrease of ΔP is gradually reduced.

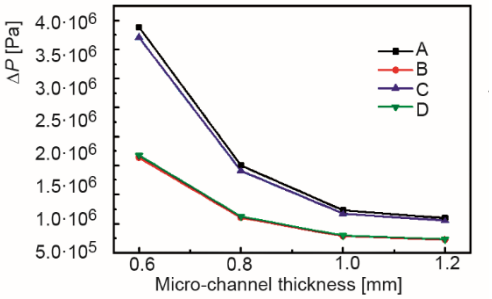

Figure 10. The variations curve of ΔP with the thickness of micro-channel under four structures

The difference of the ΔP between the structures A, C, and B, D is gradually reduced with the increase of thickness. For example, when the thickness is 0.6 mm, the difference of the ΔP between the structures A, C, and B, D reaches 2250710 Pa, while it is only 374005 Pa if the thickness of the micro-channel is increased to 1.2 mm. Hence, it can be concluded that when the micro-channel adopts a single inlet mode, considering the pressure drop from the inlet to the outlet of the cooling plate, the thickness of the micro-channel should be increased as much as possible.

The analysis of cooling performance of cold plates with different micro-channel width

The temperature distributions of the structures A, B, C, and D with different widths of micro-channel are shown in figs. 11(a)-11(d) respectively. Note that the thicknesses of micro-channels are maintained constant at 0.6 mm in all cases.

As shown in fig. 11, with the increase of the width of the micro-channel, the high temperature regions of the cold plate under the structures B, C, and D are gradually expanded, and the increasing regions are mainly concentrated in the middle of the cold plates, while the high temperature area of structure A is slightly reduced, and the reducing regions are mainly concentrated in the bottom of the cold plate. Meanwhile, as the increase of the width of the micro-channel, the low temperature regions at the inlet of the cooling liquid are gradually increased in all cases. On the hand, with the increase of the width of the micro-channel, the flow velocity of the cooling liquid is decreased, which leads to the total heat transfer efficiency of the cooling liquid is reduced, hence, the high temperature area in the middle of the cold plate is expanded. On the other hand, with the increase of the width of the micro-channel, the total fluid areas are expanded and the distances between adjacent the micro-channels are reduced at the same time, which the heat transfer areas of the cooling liquid are increased, hence, the low temperature regions at the inlet of the cooling liquid are expanded.

The variation curves of T_{max}, T_{diff}, and T_{σ} with the thickness of micro-channels are shown in figs. 12(a)-12(c) respectively. As shown in figs. 12(a) and 12(b), both T_{max} and T_{diff} are increased in all cases with the increase of the width, indicating that the most severe operating conditions of batteries are further aggravated. It is worth noting that the variations of the T_{max} and T_{diff} of structure A with the increase of the width are relatively slower than those other three structures.

When the width of the clod plate is less than 6 [mm], the T_{max} of structure A is all the highest, while the T_{max} of structure A is exceeded by structure C if the width is increased

to 7 mm. This indicates that structure C is more likely to be affected by the change of the width of micro-channel than the structure A.

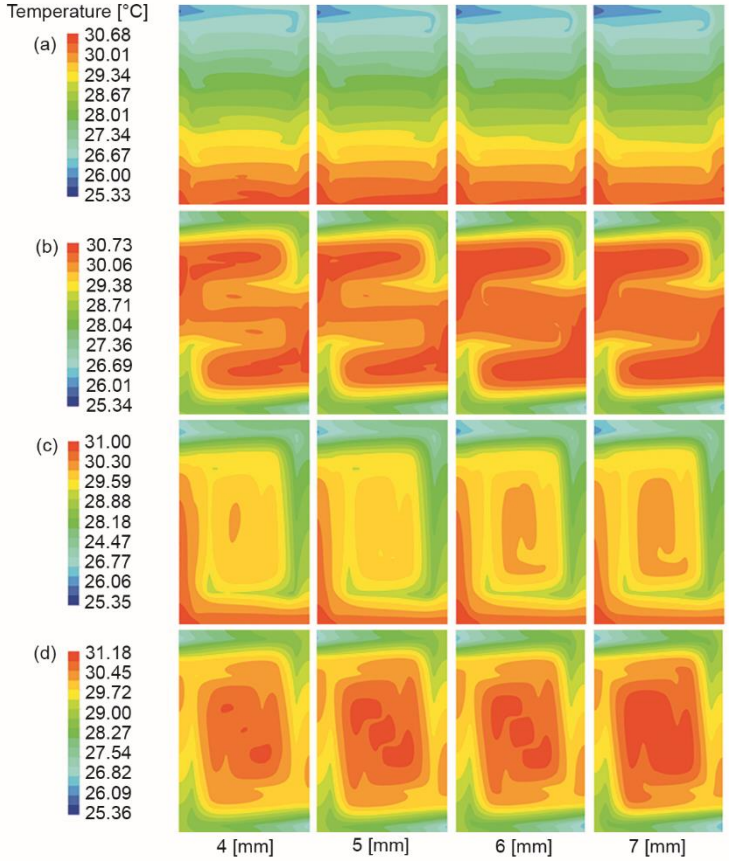

Figure 11. The temperature distributions under different widths of micro-channel (*for color image see journal web site*)

As shown in fig. 12(c), with the increase of the width of the micro-channel, the T_σ in all cases are gradually increased, similarly, the increment of the structure A is the slowest than the structures B, C, and D. The T_σ of the structure A are the highest in all cases, which indicating that structure A has poor performance in maintaining temperature uniform of the cold plate. However, for the same width, the T_σ of structure C is the lowest in all cases, which indicating that structure C can maintain the temperature uniformity of the cold plate well.

The variation curves of ΔP with the width of the micro-channels under the four structures as shown in fig. 13. It can be found that the ΔP in all cases is gradually decreased as the increases of width. This phenomenon is caused by the change of cooling liquid velocity and the equivalent diameter of the micro-channel with the increases of the width. It should be noted that the decreasing amount and changing range of ΔP caused by the change of width is smaller than caused by the change of the thickness. This phenomenon can be explained that the

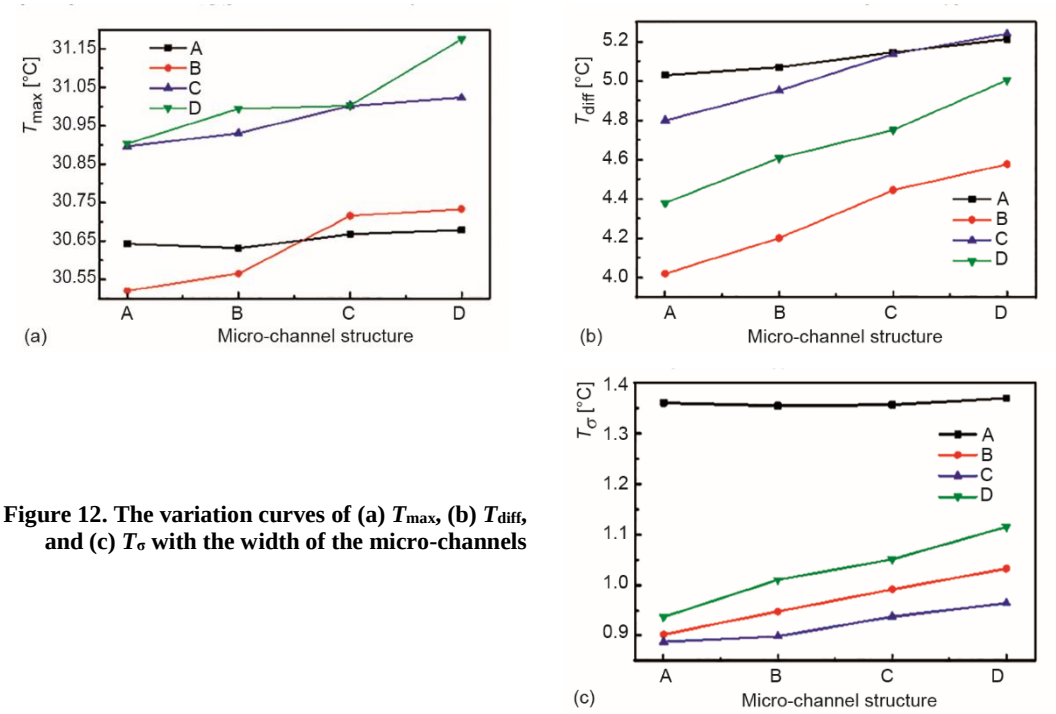

Figure 12. The variation curves of (a) T_{max}, (b) T_{diff}, and (c) T_σ with the width of the micro-channels

change of the equivalent diameter of the micro-channel is more influenced by the change of the thickness.

By comparing the change curve of ΔP of structures A and C, it should be noted that the ΔP of structure A is higher when the width is less than 6 mm, which is mainly caused by the fact that structure A has more parts that cause the cooling liquid direction to be changed, hence the local loss caused by it is greater. However, the ΔP of structure A is lower than that of structure C if the width exceeds 6 mm, which indicates that structure A is more affected by the width of the micro-channel.

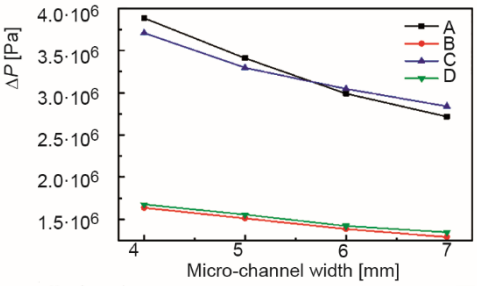

Figure 13. The variation curves of ΔP with the width of the micro-channels

Conclusions

In this paper, structures A, B, C, and D four types of the micro-channel cold plates are designed, and the effects of the changes of the thickness and width of micro-channel on the thermal management performance are studied by numerical simulation. The major conclusions are as follows.

- The temperature distribution of structure A shows a gradually rising trend from top to bottom, while that of structure B shows a characteristic that the upper and lower parts of the cold plate are lower and the middle parts of the cold plate are higher. The high temperature areas of structure C are mainly distributed at the left edge and the bottom edge

regions of the cold plate, while these of structure D are mainly concentrated in the center regions of the cold plate.

- With the increase of the thickness of the micro-channel, the T_{max} of cold plate is gradually increased under the structures A, B, and C, while it is gradually decreased under the structure D. The T_σ of the structure A is less affected by the change of the thickness of the micro-channel. The temperature uniformity of the cold plate can be well maintained when the thickness of the micro-channel is 1.0 mm under the structures B, C, and D. When the micro-channel adopts single inlet mode, considering the pressure drop from the inlet to the outlet of the cooling plate, the thickness of the micro-channel should be increased as much as possible.
- With the increase of the width of the micro-channel, the high temperature areas of the cold plate are gradually expanded under structures B, C, and D, while it is slightly reduced under structure A. The T_{max}, T_{diff}, and T_σ are gradually increased in all cases, while the ΔP from the inlet to the outlet is gradually decreased. The temperature uniformity of the cold plate is well maintained by structure A. The decreasing amount and changing range of ΔP caused by the change of micro-channel width is smaller than caused by the change of the thickness.

The results of this study will be useful for the design of a micro-channel cold plate for a large-capacity rectangular battery.

Acknowledgment

This work was funded by the Key Projects of Nanjing 321 Plan (No.2013B03004).

References

[1] Bu, C., *et al.*, Oxy-Fuel Combustion of a Single Fuel Particle in a Fluidized Bed: Char Combustion Characteristics, an Experimental Study, *Chemical Engineering Journal*, *287* (2016), Mar., pp. 649-656
[2] Fathabadi, H., A Novel Design Including Cooling Media for Lithium-ion Batteries Pack Used in Hybrid and Electric Vehicles, *Journal of Power Sources*, *245* (2014), Jan., pp. 495-500
[3] Kang, B. H., Lee, H. J., A Review of Recent Research on Automotive HVAC Systems for EV, *International Journal of Air-Conditioning and Refrigeration*, *25* (2017), 4, 1730003
[4] Wada, M., Research and Development of Electric Vehicles for Clean Transportation, *Journal of Environmental Sciences*, *21* (2009), 6, pp. 745-749
[5] Lu, L., *et al.*, A Review on the Key Issues for Lithium-Ion Battery Management in Electric Vehicles, *Journal of Power Sources*, *226* (2013), Mar., pp. 272-288
[6] Zhao, X. Y., Thermal Performance Analysis and Optimal Control of Power Lithium Cell Thermal Management System for New Energy Vehicles, *Thermal Science*, *24* (2020), 5, pp. 3375-3383
[7] Sun, X. D., *et al.*, Research On Thermal Equilibrium Performance of Liquid-Cooled Lithium-Ion Power Battery System at Low Temperature, *Thermal Science*, *24* (2020), 6, pp. 4147-4158
[8] An, Z., *et al.*, Experimental Investigation on Lithium-Ion Battery Thermal Management Based on Flow Boiling in Mini-Channel, *Applied Thermal Engineering*, *117* (2017), May, pp. 534-543
[9] Xie, J., *et al.*, Structural Optimization of Lithium-Ion Battery Pack with Forced Air Cooling System, *Applied Thermal Engineering*, *126* (2017), Nov., pp. 583-593
[10] Huo, Y., *et al.*, Investigation of Power Battery Thermal Management by Using Mini-Channel Cold Plate, *Energy Conversion and Management*, *89* (2015), Jan., pp. 387-395
[11] Wang, Z., *et al.*, Paraffin and Paraffin/Aluminum Foam Composite Phase Change Material Heat Storage Experimental Study Based on Thermal Management of Li-Ion Battery, *Applied Thermal Engineering*, *78* (2015), Mar., pp. 428-436
[12] Saw, L. H., *et al.*, Computational Fluid Dynamic and Thermal Analysis of Lithium-Ion Battery Pack with Air Cooling, *Applied Energy*, *177* (2016), Sept., pp. 783-792
[13] Fang, Y., *et al.*, Investigation on the Transient Thermal Performance of a Mini-Channel Cold Plate for Battery Thermal Management, *Journal of Thermal Science*, *30* (2020), 5, pp. 914-925

[14] Wang, J., *et al.*, Sensitivity Analysis of Factors Influencing a Heat Pipe-Based Thermal Management System for a Battery Module with Cylindrical Cells, *Applied Thermal Engineering*, *151* (2019), Mar., pp. 475-485
[15] Xia, G., *et al.*, A Review on Battery Thermal Management in Electric Vehicle Application, *Journal of Power Sources*, *367* (2017), Nov., pp. 90-105
[16] Tang, A., *et al.*, Optimization Design and Numerical Study on Water Cooling Structure for Power Lithium Battery Pack, *Applied Thermal Engineering*, *159* (2019), Aug., 113760
[17] Lee, M.-Y., *et al.*, Thermal Abuse Behavior of the LIR2450 Micro Coin Cell Battery Having Capacity of 120 mAh with Internal Short Circuit by Penetrating Element, *Symmetry*, *12* (2020), 2, 246
[18] Deng, T., *et al.*, Study on Thermal Management of Rectangular Li-Ion Battery with Serpentine-Channel Cold Plate, *International Journal of Heat and Mass Transfer*, *125* (2018), Oct., pp. 143-152
[19] Lan, C., *et al.*, Thermal Management for High Power Lithium-Ion Battery by Minichannel Aluminum Tubes, *Applied Thermal Engineering*, *101* (2016), May, pp. 284-292
[20] Dong, F., *et al.*, Investigation of the Effect of U-Shaped Mini-Channel Structure on the Thermal Performance of Liquid-Cooled Prismatic Batteries, *Numerical Heat Transfer Applications*, *77* (2019), 1, pp. 1-16

Paper submitted: June 8, 2021
Paper revised: August 27, 2021
Paper accepted: October 18, 2021